ACS APPLIED MATERIALS & INTERFACES

Research Article

www.acsami.org

Low-Temperature, Solution-Processed ZrO_2:B Thin Film: A Bifunctional Inorganic/Organic Interfacial Glue for Flexible Thin-Film Transistors

Jee Ho Park,[†] Jin Young Oh,[†,‡] Sun Woong Han,[†] Tae Il Lee,*[,§] and Hong Koo Baik*[,†]

[†]Department of Materials Engineering, Yonsei University, Seoul 120-749, Republic of Korea

[‡]Research Institute of Iron and Steel Technology, Yonsei University, 134 Shinchon-dong Seodaemun-gu, Seoul 120-749, Republic of Korea

[§]Department of BioNano Technology, Gachon University, Seongnam, Gyeonggi-Do 461-701, Republic of Korea

Supporting Information

ABSTRACT: A solution-processed boron-doped peroxo-zirconium oxide (ZrO_2:B) thin film has been found to have multifunctional characteristics, providing both hydrophobic surface modification and a chemical glue layer. Specifically, a ZrO_2:B thin film deposited on a hydrophobic layer becomes superhydrophilic following ultraviolet−ozone (UVO) treatment, whereas the same treatment has no effect on the hydrophobicity of the hydrophobic layer alone. Investigation of the ZrO_2:B/hydrophobic interface layer using angle-resolved X-ray photoelectron spectroscopy (AR XPS) confirmed it to be chemically bonded like glue. Using the multifunctional nature of the ZrO_2:B thin film, flexible amorphous indium oxide (In_2O_3) thin-film transistors (TFTs) were subsequently fabricated on a polyimide substrate along with a ZrO_2:B/poly-4-vinylphenol (PVP) dielectric. An aqueous In_2O_3 solution was successfully coated onto the ZrO_2:B/PVP dielectric, and the surface and chemical properties of the PVP and ZrO_2:B thin films were analyzed by contact angle measurement, atomic force microscopy (AFM), Fourier transform infrared (FT-IR) spectroscopy, and X-ray photoelectron spectroscopy (XPS). The surface-engineered PVP dielectric was found to have a lower leakage current density (J_{leak}) of 4.38×10^{-8} A/cm^2 at 1 MV/cm, with no breakdown behavior observed up to a bending radius of 5 mm. In contrast, the electrical characteristics of the flexible amorphous In_2O_3 TFT such as on/off current ratio ($I_{on/off}$) and electron mobility remained similar up to 10 mm of bending without degradation, with the device being nonactivated at a bending radius of 5 mm. These results suggest that ZrO_2:B thin films could be used for low-temperature, solution-processed surface-modified flexible devices.

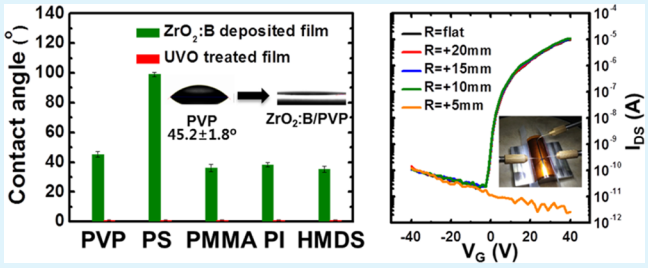

KEYWORDS: *bifunctional inorganic/organic interfacial glue, flexible electronics, solution processing, thin-film transistor, boron-doped peroxo-zirconium oxide*

1. INTRODUCTION

Solution-processed metal-oxide thin-film transistors (TFTs) have been intensively researched, because of their simple processing, low cost, and large area uniformity. Channel layers of indium gallium zinc oxide (IGZO),[1] indium zinc oxide (IZO),[2] zinc tin oxide (ZTO),[3] and zinc oxide (ZnO)[4] have all been obtained by solution processing, along with dielectric layers of zirconium oxide (ZrO_2),[5,6] hafnium oxide (HfO_2),[7] and aluminum oxide (Al_2O_3).[8] The deposition of metal oxide thin films on flexible substrates such as polyimide (PI), polyethylene terephthalate (PET), and polyethylene sulfonate (PES) requires annealing temperatures lower than 200 °C; however, an annealing temperature above 350 °C is typically needed to create a metal-oxide thin film, because of the high pyrolysis temperature of organic compounds, as well as the high activation energy of the dehydroxylation reaction.[9] Because such temperatures are incompatible with the use of a polymer substrate, many researchers have focused their efforts on reducing the annealing temperature of channel and dielectric layers to <200 °C by means of the chemical combustion of a fuel and oxidizer,[10] *in situ* hydrolysis through water vapor treatment,[11] high-density deep ultraviolet (DUV) irradiation,[12] high-pressure annealing under an O_2 atmosphere,[13] doping with suitable dopants,[6] or the use of an aqueous precursor solution.[7] However, most of these have only described the electrical properties of metal-oxide TFTs on a vacuum-deposited dielectric layer.

To achieve solution-processed metal-oxide TFTs, both the channel and dielectric layers should be deposited through a solution process. Moreover, a polymer is more desirable for the dielectric layer than an inorganic material, as far as flexibility is concerned, as the van der Waals bonding of polymers results in

Received: August 21, 2014
Accepted: February 9, 2015
Published: February 9, 2015

ACS Publications © 2015 American Chemical Society

DOI: 10.1021/acsami.5b00036
ACS Appl. Mater. Interfaces 2015, 7, 4494−4503

a low Young's modulus. In contrast, the high Young's modulus created by the strong covalent or ionic bonds of a metal oxide thin film can easily cause it to crack under even a small applied strain. Moon et al. successfully fabricated a ZnO TFT on a PES substrate using an organic−inorganic hybrid dielectric, resulting in an electron mobility of 0.033 $cm^2/(V\ s)$.[14] Similarly, Yang et al. reported a ZnO TFT on a polyarylate substrate with a poly(2-hydroxyethyl methacrylate) dielectric, which produced an electron mobility of 1.1 $cm^2/(V\ s)$ and an on/off current ratio ($I_{on/off}$) of 10^3.[15] However, both examples were of polycrystalline ZnO TFTs on a plastic substrate, with the electrical properties measured under flat conditions.[10,16−19]

In order to achieve flexible TFTs on a polymer substrate and evaluate their bending properties, we adopted a polymer dielectric and an inorganic thin film that served as an interface-engineered layer between the polymer dielectric and the channel layer. As most organic thin films have a naturally hydrophobic surface that makes it difficult to deposit an aqueous precursor solution, an interface-engineered layer with a hydrophilic surface is needed to allow spin-coating of the channel layer from an aqueous precursor solution. The requirements of this inorganic thin-film interface-engineered layer were a high degree of smoothness, a high oxidation state with a low concentration of hydroxyl groups, and a hydrophilic surface. The smooth surface ensures reduced electron scattering at the channel/dielectric interface,[20] whereas the high oxidation state leads to a reduction in electron trap sites,[21] because of the fact that hydroxyl groups created by imperfect dehydroxylation are typically quite prominent electron trap sites. In the case of SiO_2, this electron trapping mechanism is believed to involve the following reactions:

$$\equiv Si-O-Si \equiv + H_2O \leftrightarrow 2SiOH$$

$$\equiv Si-OH + H_2O \leftrightarrow SiO^- + H_3O^+$$

$$\equiv Si-O^- + H_3O^+ + e^- \leftrightarrow SiO^- + H_2O + \frac{1}{2}H_2$$

Note that hydroxyl groups encountering H_2O molecules produce a negative charge, along with protons that capture electrons and release hydrogen gas. The high acidity of the hydroxyl groups accelerates the forward reaction, which, in turn, leads to electron trapping; thus, a metal oxide thin film containing a high ratio of M−O bonds with a low number of hydroxyl groups can reduce the number of electron trap sites.[22]

Several groups have previously described inorganic/organic bilayer or hybrid gate dielectrics for flexible oxide TFTs. For instance, Yoon et al. created a Li-ZnO TFT with YO_x/polyimide gate dielectric at 300 °C on a glass substrate,[23] while Yoo et al. achieved a ZnO TFT on an alumina/polyimide gate dielectric at 230 °C that had a mobility of 0.11 $cm^2/(V\ s)$.[24] Son et al. reported vacuum-deposited IZO TFT on a solution-processed ZrO_2 doped PVP-*co*-PMMA dielectric at 250 °C.[25] However, although these studies succeeded in producing metal oxide TFTs with inorganic/organic bilayer or hybrid gate dielectrics, they relied on using rigid substrates. Furthermore, to date, there has been only very few studies on the bending characteristics of flexible TFTs.[26,27]

We have previously fabricated an organic TFT with a poly(4-vinylphenol) (PVP)/yttrium oxide (YO_x) dielectric,[28] in which the PVP thin film was used to change the YO_x thin-film surface from hydrophilic to hydrophobic, because its surface hydroxyl groups result in an inferior channel/dielectric interface and poor crystalline growth of the pentacene channel. More recently, we developed a boron-doped peroxo-zirconium oxide (ZrO_2:B) dielectric at 200 °C that consisted of a dense film with a very smooth surface,[6] which was found to have a refractive index of 1.8, a leakage current density (J_{leak}) of 2.2×10^{-6} A/cm^2 at 1 MV/cm, and a breakdown voltage of 3.94 MV/cm. These characteristics were attributed to the presence of peroxo groups, the boron dopant, and the low dehydroxylation temperature of boron hydroxide.

In this study, we explore the possibility of using a ZrO_2:B thin film as an inorganic glue and surface modifier for a variety of hydrophobic layers such as cross-linked poly-4-vinylphenol (PVP), polystyrene (PS), poly(methyl methacrylate) (PMMA), polyimide (PI), and hexamethyldisiloxane (HMDS). Angle-resolved X-ray photoelectron spectroscopy (AR-XPS) confirmed that the ZrO_2:B thin film chemically bonds with the hydrophobic thin film as an inorganic glue, while ultraviolet−ozone (UVO) treatment was used to make the ZrO_2:B-coated hydrophobic thin film superhydrophilic. Finally, a PVP layer was combined with the ZrO_2:B thin film to produce a flexible amorphous indium oxide (In_2O_3) TFT. This In_2O_3 TFT was successfully operated on heavily boron-doped silicon (p^{++} Si) and PI substrates at 200 °C, and its surface characteristics were analyzed by contact angle measurement, FT-IR, XPS, and AFM. The ZrO_2:B thin film exhibited a J_{leak} value of 4.38×10^{-8} A/cm^2 at 1 MV/cm, and did not show any evidence breakdown behavior up to 100 V under convex and concave bending conditions of 5 mm. In fact, the electrical properties of the flexible TFT remained uniform up to a 10 mm convex and concave bending condition, becoming inactive at the 5-mm bending condition. This reveals that ZrO_2:B is suitable for use as a PVP surface engineering layer. In addition, an amorphous In_2O_3 channel layer leads to very uniform electrical characteristics up to a 10-mm bending condition.

2. EXPERIMENTAL SECTION

2.1. Solution Preparation. The In_2O_3 solution used was made by adding 0.1 M of indium nitrate hydrate to deionized water. For the ZrO_2:B solution, zirconium oxychloride octahydrate with 9 mol % boric acid and 6.67 M of hydrogen peroxide was mixed with 2-methoxyethanol. The PVP precursor solution was prepared by mixing poly(4-vinylphenol), poly(melamine-*co*-formaldehyde) methylated as a cross-linker, and propylene glycol monomethyl ether acetate (PGMEA) at a ratio of 10:1:1 by weight. Details of this experimental method have been described previously.[6,28] For the PS and PMMA solutions, 20 wt % of PS and PMMA were dissolved separately in chlorobenzene. The PI solution was provided by LG Display, and the HMDS solution was purchased from Sigma−Aldrich. Prior to spin coating, all solutions were stirred for 24 h, and then filtered through 0.2 μm polytetrafluoroethylene (PTFE) syringe filters.

2.2. Film Characterization. Contact angles were measured using a contact angle analyzer (Model Phoenix200, SEO) with deionized (DI) water, and the surface roughness was examined by atomic force microscopy (AFM) (Model XE100, psia). The molecular vibration of the as-deposited and cross-linked PVP was investigated by attenuated total reflectance Fourier transform infrared spectroscopy (ATR-FT IR) (Model Vertex 70, Bruker) in the range of 500−4000 cm^{-1}. The chemical state of the ZrO_2:B film was measured by X-ray photoelectron spectroscopy (XPS) (K-alpha, Thermo UK) using Al Kα radiation (1486.6 eV), with a C 1s peak at 284.8 eV used for calibration. The film thickness was measured by field-emission scanning electron microscopy (FE-SEM) (Model JSM-7001F, JEOL) and spectroscopic ellipsometry (Model SE MG-Vis 1000, Nano View). TEM image of In_2O_3/ZrO_2:B interface was obtained with the high-resolution transmission electron microscopy (HRTEM) (Model JEM ARM 200F, JEOL).

DOI: 10.1021/acsami.5b00036
ACS Appl. Mater. Interfaces 2015, 7, 4494−4503

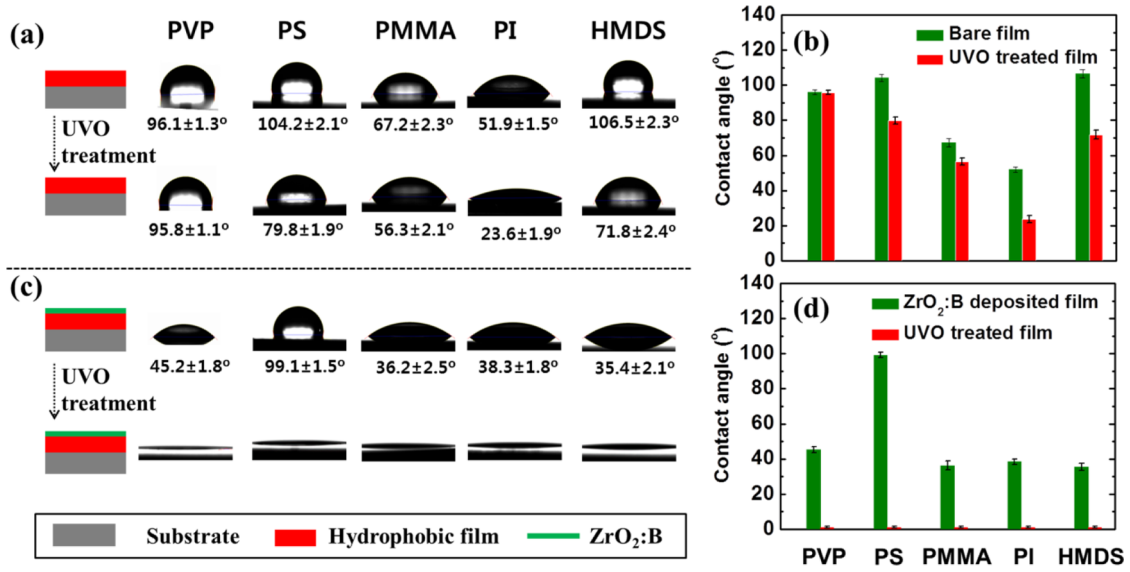

Figure 1. (a) WCA of various hydrophobic thin films before and after UVO treatment; a summary of these values is shown in panel (b). (c) WCA of various hydrophobic layers that were surface-modified by a ZrO_2:B thin film, before and after UVO treatment; a summary of these values is shown in panel (d).

2.3. Metal/Insulator/Metal Device Fabrication. The dielectric properties were evaluated using metal/insulator/metal (MIM) structures with a 0.17 mm^2 circular Al electrode. For this, the p^{++} Si substrate was first cleaned by piranha solution (H_2SO_4:H_2O_2 = 3:1) for 15 min, then washed twice in DI water for 10 min each time. The PI substrate was cleaned by acetone, isopropyl alcohol, and DI water for 10 min in each solution, and then preheated at 200 °C for 1 h. The PVP thin films were applied to each substrate by spin-coating at 3000 rpm for 50 s, following which they were annealed at 200 °C for 1 h. Next, ZrO_2:B thin films were applied by spin-coating at 3000 rpm for 20 s, which were then annealed at 200 °C for 1 h. Finally, an Al electrode was deposited by thermal evaporation with a shadow metal mask.

2.4. Thin-Film Transistor Device Fabrication. Interface-engineered In_2O_3 TFTs were fabricated on heavily boron-doped silicon (Si^{2+}) and PI substrates, with both TFTs having a bottom-gate top-contact structure. In the case of an In_2O_3 TFT on a Si^{2+} substrate, the PVP layer was spin-coated at 3000 rpm for 50 s, then annealed at 200 °C for 1 h. Next, a ZrO_2:B interface-engineered layer was deposited at 3000 rpm for 20 s and annealed at 200 °C for 1 h. To render the ZrO_2:B film superhydrophilic, UVO treatment was conducted for 10 min. The UVO treatment did not change structural and chemical state of ZrO_2:B thin film (see Figure S1 in the Supporting Information). Finally, an In_2O_3 film was spin-coated at 3000 rpm for 20 s and then annealed at 200 °C for 2 h to provide a channel layer. In the case of an In_2O_3 TFT on a PI substrate, PVP was deposited at 3000 rpm for 50 s and then annealed at 200 °C for 1 h to provide a planarization layer. An aluminum gate electrode with a thickness of 30 nm was then deposited by means of a thermal evaporator through a shadow metal mask. Following this, an In_2O_3/ZrO_2:B/PVP layer was deposited in the same manner as the p^{++} Si substrate. An Al source/drain electrode 50 nm in thickness was also deposited by a thermal evaporator through a shadow metal mask. The resulting channel length and width were 150 and 1500 μm, respectively.

2.5. Electrical Measurements. The capacitance of the PVP and ZrO_2:B/PVP films was measured by a Model HP 4284A LCR meter (Agilent) in a frequency range from 20 Hz to 1 MHz for both p^{++} Si and PI substrates. The leakage current characteristics of PVP and ZrO_2:B/PVP films on PI substrates were measured by a semiconductor parameter analyzer (Agilent, Model E5270) with a 50-nm-thick circular Al electrode. This same device was used to measure the electrical properties (in darkness) of In_2O_3 TFTs on PVP/Si^{2+}, ZrO_2:B/PVP/Si^{2+}, and ZrO_2:B/PVP/Al/PVP/PI substrates at room temperature. The bending properties were investigated using a custom-built bending tester, with a bending radius varying from a flat state to a deviation of 5 mm.

3. RESULTS AND DISCUSSION

3.1. Bifunctional Inorganic/Organic Interfacial Glue Layer. Unlike vacuum deposition, solution processing is very sensitive to the surface properties of the material being coated. In particular, a hydrophobic surface can result in the aqueous solution being readily dewetted, because of its high surface tension, thus making it necessary to alter the surface to one that is more hydrophilic. Having recently identified that a ZrO_2:B thin film can provide the necessary surface modification layer, we investigated the water contact angle (WCA) created when it is applied to commonly used hydrophobic materials such as PVP, PS, PMMA, PI, and HMDS. All these hydrophobic materials were spin-coated at 3000 rpm for 50 s onto silicon substrates and then annealed at 200 °C for 1 h; their surface characteristics are modified through UVO treatment for 40 min.

Figure 1 shows the WCA of the hydrophobic materials before and after UVO treatment, in which we see that the PVP, PS, and HMDS thin films all had a high WCA of >90°, whereas the PMMA and PI thin films were both ∼60°. However, with the exception of the PI thin film, there was no notable change in the WCA with UVO treatment that would allow an aqueous solution to be deposited without a surface modification layer. On the other hand, when a ZrO_2:B hydrophobic layer was applied, a relatively low WCA of <50° (Figure 1c) was observed with all but the PS thin film; the high WCA of the ZrO_2:B coated PS most likely being caused by a rough surface morphology (see Figure S2 in the Supporting Information). More importantly, after UVO treatment, all of the ZrO_2:B coated hydrophobic layers became superhydrophilic, with a WCA of 1° .The WCA values are summarized in Figure 1d, which clearly shows the importance of the ZrO_2:B thin film to achieving a superhydrophilic surface.

DOI: 10.1021/acsami.5b00036
ACS Appl. Mater. Interfaces 2015, 7, 4494−4503

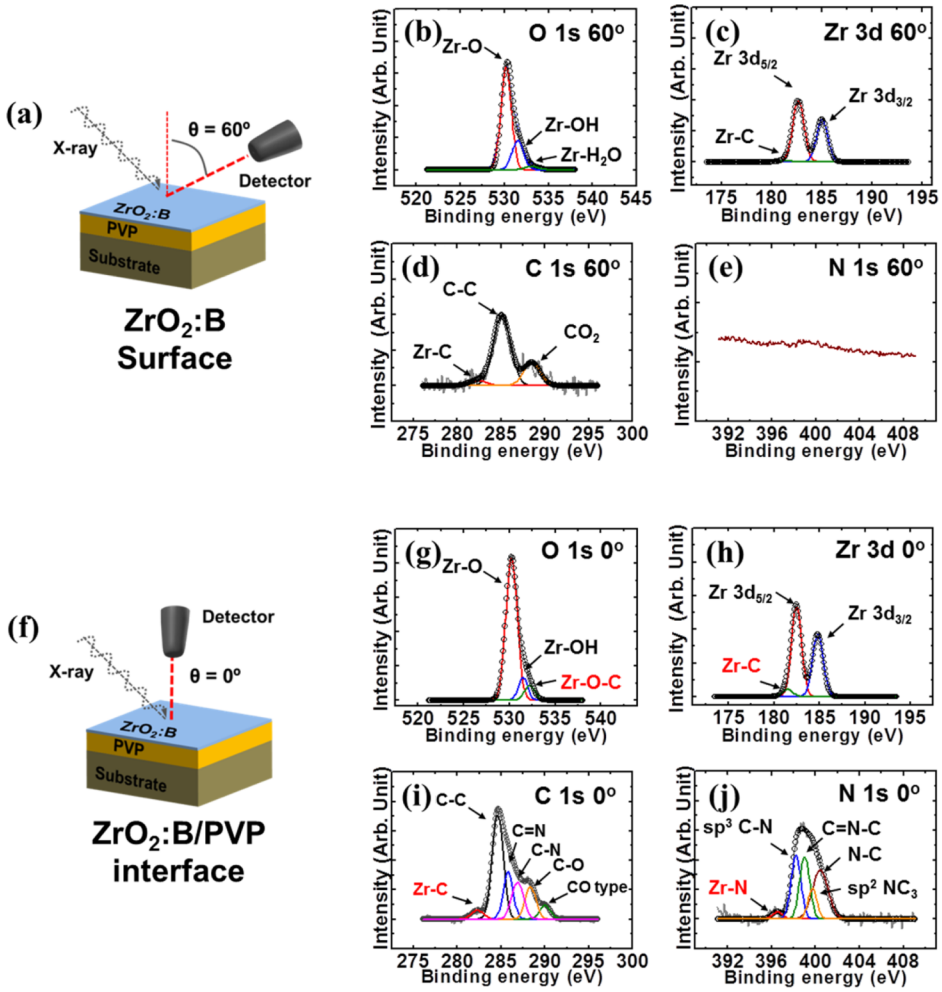

Figure 2. (a) Schematic illustration of AR-XPS measurement at a take-off angle of 60° to determine the surface state of ZrO_2:B. (b–e) The O 1s (panel (b)), Zr 3d (panel (c)), C 1s (panel (d)), and N 1s (panel (e)) spectra obtained at 60°. (f) Schematic illustration of AR-XPS measurement at a takeoff angle of 0° to determine the ZrO_2:B/PVP interface state. (g–j) The O 1s (panel (g)), Zr 3d (panel (h)), C 1s (panel (i)), and N 1s (panel (j)) spectra obtained at a take-off angle of 0°.

In addition to changing the surface properties, it is also important that the surface modification layer form a strong chemical bond with the hydrophobic film. To identify the nature of the bond at the ZrO_2:B/hydrophobic layer interface, we used a conventional PVP layer as the hydrophobic gate insulator and created a thin ZrO_2:B film by diluting the ZrO_2:B solution four times and coating at 6000 rpm for 20 s. Through spectroscopic ellipsometry, the thickness of this film was measured as 2 nm, and the results of its subsequent analysis by AR XPS at a take-off angle of 60° are shown in Figure 2. The binding energy and corresponding phases are summarized in Table S1 in the Supporting Information. These data reveal that the ZrO_2:B was well-formed, with a high ratio of Zr–O to Zr–OH. Water and CO_2 adsorption are evidenced by the O 1s peak (533 eV) and the C 1s peak (288.5 eV), respectively, but only very small Zr–C and C–C peaks are observed due to the thinness of the ZrO_2:B film. Furthermore, no N 1s peaks associated with the PVP cross-linker can be observed. In order to identify the bonding type present in the ZrO_2:B/PVP interface, XPS data were also acquired at a take-off angle of 0° (Figure 2d). This analysis found well-defined peaks for Zr–O–C, Zr–C, and Zr–N that all directly indicate a chemical bond between ZrO_2:B and PVP at the interface. Therefore, it is concluded that the ZrO_2:B thin film has bifunctional properties, providing both an inorganic hydrophobic surface modification layer and a gluelike chemical bonding layer.

3.2. Characterization of ZrO_2:B/PVP Thin Film. For the purposes of this study, a PVP layer was chosen as the flexible gate dielectric on the basis that this material is already commonly used in organic TFTs; however, the hydrophobic surface created by its vinyl functional group requires that a hydrophilic surface be applied prior to depositing aqueous In_2O_3 solutions for the channel layer. Typically, UVO treatment has been used to form hydroxyl groups on the film surface and render it hydrophilic, but this can damage the surface and change the polymer structure. Therefore, we used optical microscopy (OM) and SEM images of the PVP layer before and after UVO treatment (Figure S3 in the Supporting Information) to determine the extent of any damage caused. A comparison between the contact angle of PVP and a UVO-treated PVP thin film is shown in Figures 1a and 1c, with the fact that both films have almost the same contact angle of 96° confirming that UVO treatment does not, in fact, produce hydroxyl groups on the PVP thin film surface. In the case of a ZrO_2:B/PVP thin film, on the other hand, the contact angle changes from 45° to 1° after UVO treatment (Figure 1c). This indicates that (i) the ZrO_2:B thin film was well-deposited on

DOI: 10.1021/acsami.5b00036
ACS Appl. Mater. Interfaces 2015, 7, 4494–4503

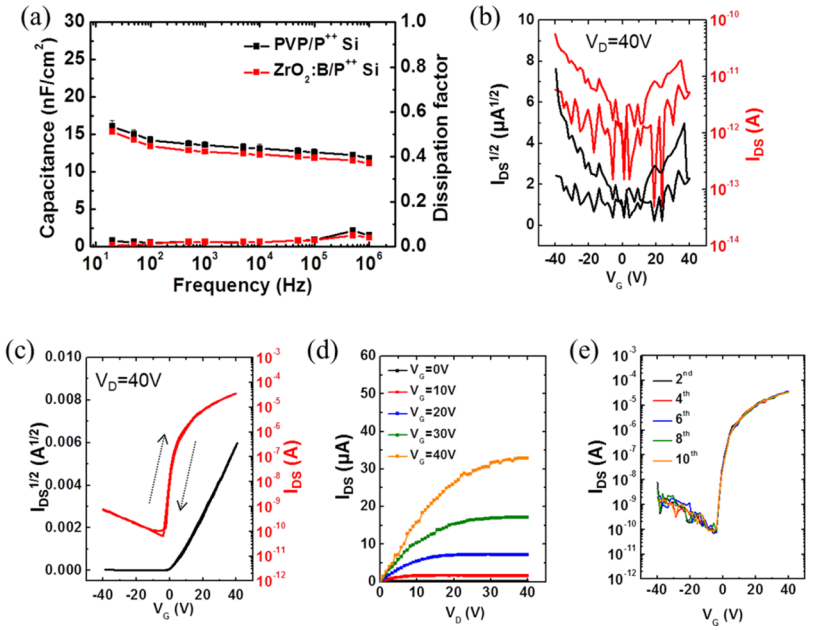

Figure 3. (a) Capacitance and dissipation factors of PVP and ZrO_2:B/PVP dielectrics on a p^{++} Si substrate across the entire frequency range. (b) Transfer curves of an In_2O_3 TFT on a p^{++} Si substrate with a PVP dielectric. (c) Transfer curve, (d) output curve, and (e) 10 consecutive sweep operations for a In_2O_3 TFT on a p^{++} Si substrate with a ZrO_2:B/PVP dielectric.

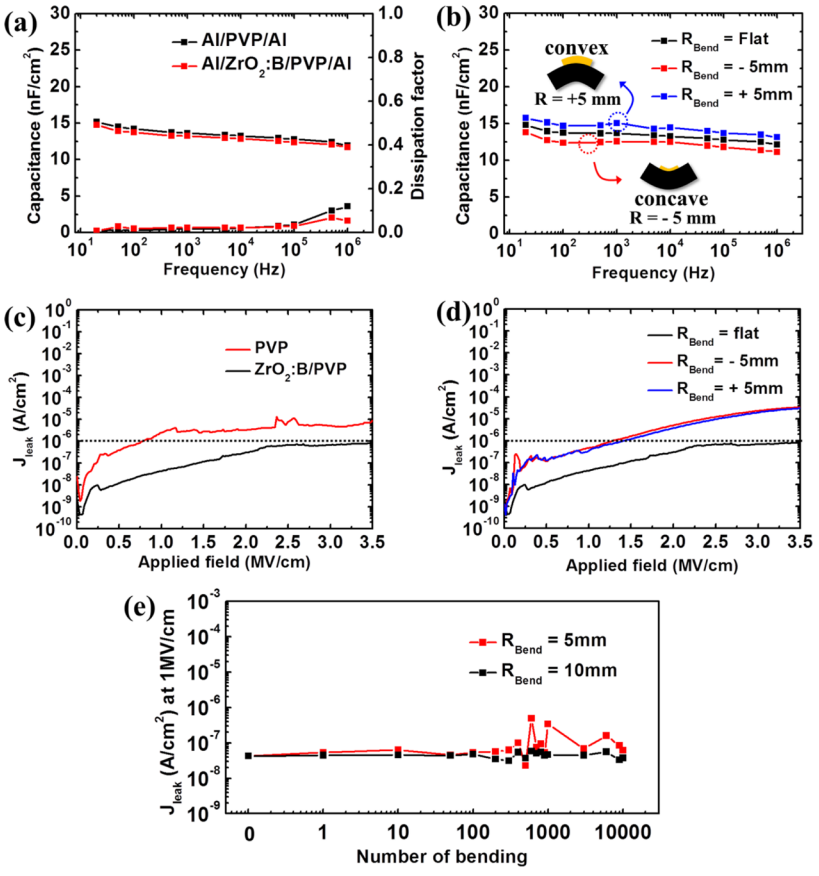

Figure 4. (a) Capacitance and dissipation factors of PVP and ZrO_2:B/PVP thin films in the 20−1 MHz range. (b) Capacitance of a ZrO_2:B/PVP thin film under convex and concave bending conditions of 5 mm. (c) J_{leak}−applied field curves of PVP and ZrO_2:B/PVP thin films. (d) J_{leak} of a ZrO_2:B/PVP thin film under convex and concave bending conditions with a bending radius of 5 mm. All devices were fabricated on a PI substrate. (e) Bending cycle test of ZrO_2:B/PVP thin film under 10 mm and 5 mm convex bending radius up to 10 000 times.

the PVP layer (see Figure S1 in the Supporting Information), and (ii) sufficient hydroxyl groups were generated.

The chemical state of the PVP thin film was investigated by FT-IR, with Figure S4a in the Supporting Information showing

DOI: 10.1021/acsami.5b00036
ACS Appl. Mater. Interfaces 2015, 7, 4494−4503

the FT-IR spectra of as-deposited and cross-linked PVP thin films. It is apparent from this that the as-deposited PVP film contains a large amount of unreacted hydroxyl groups, as evidenced by the 3000−3500 cm^{-1} vibration;[29] whereas, because of a cross-linking reaction, the 200 °C annealed PVP thin film had very few hydroxyl groups. This confirms that an annealing temperature of 200 °C is sufficient to form a PVP thin film without any significant degradation.

The chemical state of the ZrO_2:B thin film was analyzed by XPS, and its individual peaks are shown in Figure S4b in the Supporting Information. The Zr 3d signal was divided into two peaks, centered at 182.4 and 184.8 eV, which correspond to the Zr $3d_{5/2}$ and Zr $3d_{3/2}$ states, respectively.[30] The Zr $3d_{5/2}$ state indicates complete oxidation of Zr^{4+}, while Zr $3d_{3/2}$ represents spin−orbit splitting. Meanwhile, the O 1s can be deconvoluted into two peaks centered at 530.28 and 531.8 eV, which are equivalent to the fully oxidized state of Zr−O and the chemisorbed hydroxyl groups of Zr−OH, respectively.[31] The ratios of Zr−O and Zr−OH in the O 1s peaks were 0.852 and 0.148, respectively, which means that the ZrO_2:B thin film consisted mostly of Zr−O, with only a small amount of hydroxyl groups. The high ratio of Zr−O in the ZrO_2:B thin film originated from peroxo-groups and the low dehydroxylation temperature of the boron dopant.[6] In addition, the presence of both the boron dopant (centered at 192.2 eV) and residual chlorine (centered at 197.8 eV) were also confirmed.[32,33] No carbon peak was detected, however, indicating that the solvent was completely pyrolyzed at 200 °C. On the basis of these results, it can be concluded that the ZrO_2:B thin film forms Zr−O bonds at 200 °C, and that this is a sufficient temperature to ensure that the interface-engineered layer and PVP thin film are sufficiently cross-linked without degradation.

3.3. In_2O_3 TFT with ZrO_2:B/PVP Dielectric on a Si Substrate. By using ZrO_2:B as a surface modifying inorganic glue layer, a In_2O_3 TFT was fabricated on a Si substrate; the dielectric characteristics of the ZrO_2:B/PVP thin film having first been measured on a p^{++} Si substrate. Figure 3a shows the capacitance−frequency curves of the PVP and ZrO_2:B/PVP dielectric in the 20−1 MHz range, in which all capacitance values were measured at zero bias across the entire frequency range. The capacitance values of the PVP and ZrO_2:B/PVP at 20 Hz were 16.03 ± 0.78 and 15.36 ± 0.12, respectively, with both films exhibiting a low dissipation factor of <0.1 across all frequencies. The dielectric constants of the PVP and the ZrO_2:B/PVP films were 4.6 and 8.5, respectively.

Figure 3b shows a transfer curve for an In_2O_3 TFT on a p^{++} Si substrate with a PVP dielectric at a drain voltage (V_D) of 40 V. Note that this does not show semiconductor characteristics, because the In_2O_3 thin film was derived from an aqueous In_2O_3 solution that could not be formed on a hydrophobic PVP thin film. Thus, in order to obtain an In_2O_3 TFT on a PVP dielectric, the surface of the PVP thin film must be changed from hydrophobic to hydrophilic. Figure 3c shows the transfer curve of an In_2O_3 TFT on a p^{++} Si substrate with a surface-modified PVP dielectric, which was formed by inserting a ZrO_2:B thin film. This TFT has an electron mobility (μ_{sat}) of 0.44 $cm^2/(V\ s)$, a threshold voltage (V_{th}) of 1.7 V, an on/off current ratio ($I_{on/off}$) of 5.07×10^5, and a hysteresis of 0.61 V. The output curve for this TFT is shown in Figure 3d, revealing a maximum saturation current of 32.8 μA. Figure 3e shows the transfer curves obtained from 10 consecutive sweeps, which demonstrates that this In_2O_3 TFT also has good operating stability.

3.4. Dielectric Characteristics of ZrO_2/PVP on a PI Substrate. To evaluate the flexible PVP and ZrO_2:B/PVP dielectrics, we fabricated a MIM structure on a PI substrate. The capacitance−frequency data in Figure 4a shows that the capacitance of the PVP and ZrO_2:B/PVP dielectrics at 20 Hz were 15.2 ± 0.18 and 14.8 ± 0.12 nF/cm^2, respectively. Furthermore, both thin films have a low dissipation factor of <0.2 across the entire frequency range tested (20 Hz to 1 MHz). The bending properties of the ZrO_2:B/PVP dielectric were subsequently measured under convex and concave conditions, with a bending radius of 5 mm (Figure 4b). In the case of convex bending, the capacitance was slightly increased from 14.8 nF/cm^2 to 15.8 nF/cm^2; whereas under concave bending, the capacitance decreased slightly from 14.8 nF/cm^2 to 13.8 nF/cm^2. This tendency can be explained by the change in film thickness that is created by the Poisson effect; i.e., since the permittivity is only negligibly changed up until a strain of 2%, the deformation factor of the device is determined solely by its thickness. The variation in film thickness with bending can be determined from the capacitance (C), which is defined by the equation

$$C = \frac{\varepsilon A}{d}$$

where ε is the permittivity, A the area, and d the film thickness. In the case of convex bending, the film thickness decreases from 285 nm to 268 nm, whereas concave bending experiences an increase in film thickness from 285 nm to 302 nm.

The most important dielectric factor is the J_{leak} value, which should be lower than 10^{-6} A/cm^2 at 1 MV/cm if the film is to be used as a gate dielectric. Figure 4c gives J_{leak} values for PVP and ZrO_2:B/PVP thin films on a PI substrate, from which it can be seen that, although conventional PVP films greater than 300 nm in thickness successfully restrict the value of J_{leak} to $<10^{-6}$ A/cm^2 at 1 MV/cm, a 260-nm-thick film has a relatively high J_{leak} value of 2.4×10^{-6} A/cm^2 at 1 MV/cm. In contrast, a ZrO_2:B/PVP thin film effectively limits J_{leak} to a value of 4.2×10^{-8} A/cm^2 at 1 MV/cm, with no evidence of breakdown behavior, even at voltages up to 100 V. This low J_{leak} value may result from the high oxidation state and low number of defect sites within the ZrO_2:B thin film. Previous analysis of ZrO_2:B thin films with various tools[6] has found that its peroxo-groups produce low defect levels, while a boron dopant helps to form a dense film. Moreover, residual chlorine in the ZrO_2:B thin film (Figure S4b in the Supporting Information) may reduce defect sites by reducing charge trapping, decreasing fixed charge, and passivating oxygen vacancy, which is the main conduction path. Thus, as the Cl ion bonds with uncoordinated Zr ions, the oxygen vacancy may decrease bring about low J_{leak} values. We can therefore conclude that the ZrO_2:B thin film plays a dual-function role in providing both a surface-engineered and J_{leak}-enhancing layer.

To evaluate the ZrO_2:B/PVP thin film's potential as a flexible dielectric, its J_{leak} value was measured under bending conditions with a radius of 5 mm, the results of which are shown in Figure 4d. This reveals that not only does the ZrO_2:B/PVP thin film fail to exhibit any breakdown phenomenon with a bending radius of 5 mm, but it also has a lower J_{leak} value than a flat PVP thin film at 1 MV/cm. The J_{leak} values of the ZrO_2:B/PVP thin film under 5 mm convex and concave bending conditions are 3.47×10^{-7} and 4.59×10^{-7} A/cm^2 at 1 MV/cm, respectively. The cyclic bending test was performed up to 10 000 times under 5 and 10 mm concave bending conditions, and the result

DOI: 10.1021/acsami.5b00036
ACS Appl. Mater. Interfaces 2015, 7, 4494−4503

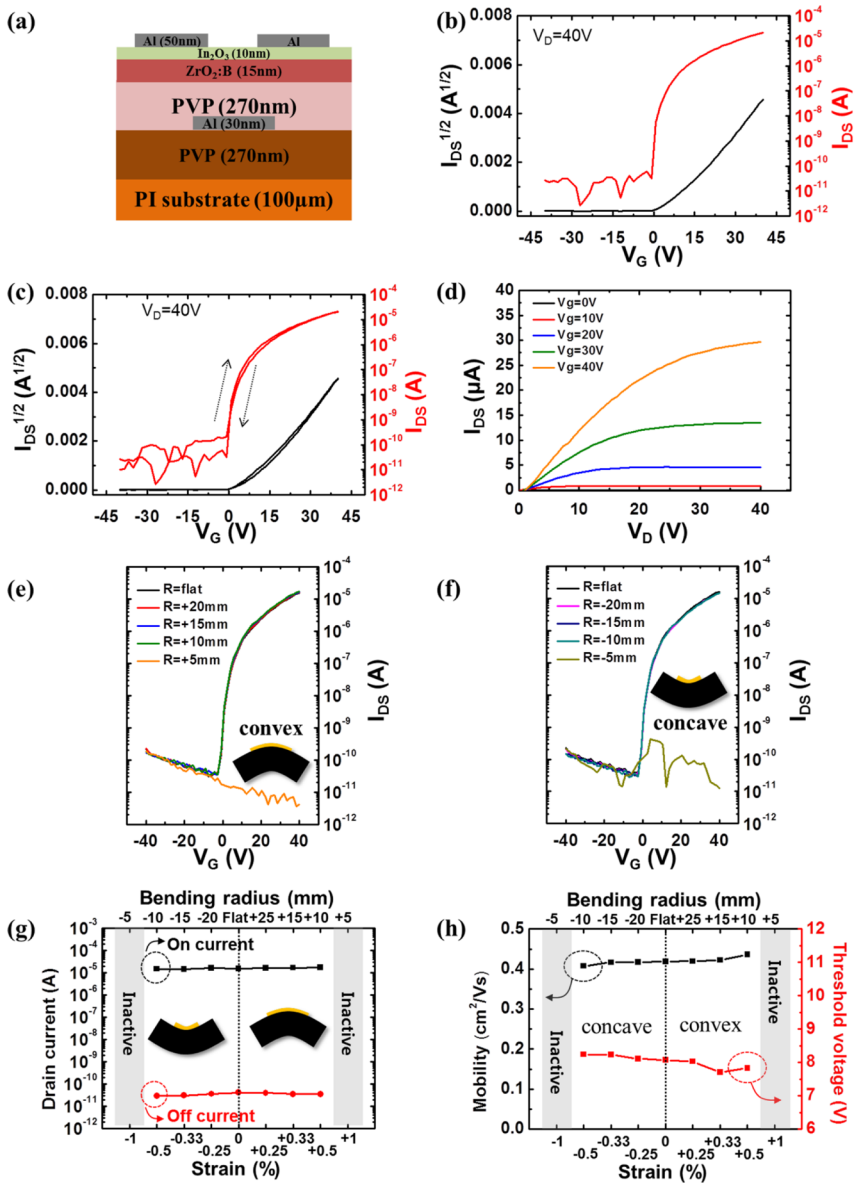

Figure 5. (a) Schematic illustration of a surface-modified flexible In_2O_3 TFT and its (b) transfer, (c) hysteresis, and (d) output curves. Transfer curves of a flexible In_2O_3 TFT under (e) convex and (f) concave bending conditions, as a function of the bending radius. Also shown are the (g) on/off current and (h) electron mobility and threshold voltage under various bending conditions.

is shown in Figure 4e. J_{leak} at 1 MV/cm exhibited a value of $<10^{-6}$ A/cm^2 in all cases. It is therefore clear that a ZrO_2:B/PVP dielectric can be used as a flexible TFT under bending conditions of up to 5 mm.

3.5. Flexible In_2O_3 TFT with ZrO_2/PVP on the PI Substrate. Finally, we fabricated a flexible TFT and evaluated its electrical properties under various bending conditions. A schematic illustration of the surface-engineered flexible amorphous In_2O_3 TFT in question is shown in Figure 5a, in which the thicknesses of the PVP, ZrO_2:B, and In_2O_3 layers are 270, 15, and 10 nm, respectively; while the thicknesses of the Al gate and source/drain electrodes are 30 and 50 nm, respectively. Examination of the surface roughness of the deposited layer by AFM found the cleaned PI substrate to have a very rough surface, with a root-mean-square (rms) value of 3.560 nm (see Figure S5a in the Supporting Information). Following spin coating of the PVP thin film, the surface became much smoother, with an rms surface roughness of 0.293 nm (see Figure S5b in the Supporting Information). As the process progressed, the surface roughness continued to decrease from 0.281 nm to 0.141 nm (see Figures S5c–e in the Supporting Information). The smooth In_2O_3/ZrO_2:B interface was also verified by HRTEM (see Figure S6 in the Supporting Information). This confirms that the PVP thin film can also provide a planarization layer, and that the ZrO_2:B surface-modification layer was well-formed with a smooth surface.

A flexible In_2O_3 TFT was subsequently fabricated on a PI substrate with a ZrO_2:B/PVP dielectric at 200 °C. The transfer curves of this flexible TFT at V_D = 40 V are shown in Figure 5b, revealing it to have values of μ_{sat} = 0.42 cm^2/(V s), V_{th} = 8.07 V, and $I_{on/off} = 3.69 \times 10^5$, which are all indicative of a reasonable electron mobility and switching ability. Figure 5c shows the hysteresis of the flexible TFT, with a value of 1.02 V obtained with a clockwise hysteresis direction. This indicates that the ZrO_2:B/PVP layer did not contain mobile ions, which cause a counterclockwise direction,[8,34,35] which can be attributed to the

DOI: 10.1021/acsami.5b00036
ACS Appl. Mater. Interfaces 2015, 7, 4494−4503

fact that the ZrO_2:B has a high oxidation state and the PVP layer is well cross-linked. The output curves shown in Figure 5d also indicate a hard saturation current, which reaches a maximum of 29.6 μA. The bending properties were investigated using a custom-built tester with various radii of curvature from 20 mm to 5 mm; Figures 5d and 5e show the transfer curves of a flexible TFT, as a function of convex bending radius, while Figure 5f shows the transfer curves with various concave bending radii. The electrical parameters are summarized in Table 1 and show little change up to a bending radius of 10 mm. No semiconductor characteristics were observed at a bending radius of 5 mm due to crack formation, and to investigate the origin of this cracking, the surface of the ZrO_2:B/PVP and In_2O_3/ZrO_2:B/PVP layers were observed by SEM. From the results shown in Figure S7 in the Supporting Information, it is evident that the crack is not formed in the ZrO_2:B/PVP layer, but rather in the In_2O_3/ZrO_2:B/PVP layer. This 20-nm-wide crack was also observed by AFM (see Figure S7c in the Supporting Information), from which it is evident that the deterioration of the flexible TFT under 5 mm of bending is the result of cracking of the channel layer. The strain (ε) was calculated using the following formula:[27]

Table 1. Electrical Properties of a Flexible In_2O_3 TFT under Various Bending Conditions

type	bending radius (mm)	strain (%)	mobility ($cm^2/(V\ s)$)	V_{th} (V)	$I_{on/off}$
convex	5	+1	inactive	inactive	inactive
	10	+0.5	0.405	8.44	5.11×10^5
	15	+0.33	0.416	8.27	4.79×10^5
	20	+0.25	0.418	8.11	4.53×10^5
flat	infinite	0	0.419	8.07	3.69×10^5
concave	20	−0.25	0.418	8.03	4.11×10^5
	15	−0.33	0.414	7.67	4.79×10^5
	10	−0.5	0.397	7.43	4.91×10^5
	5	−1	inactive	inactive	inactive

$$\varepsilon = \frac{d}{2R}$$

where d is the substrate thickness and R is the bending radius. Thus, bending radii of 20, 15, 10, and 5 mm correspond to ε values of 0.25%, 0.33%, 0.5%, and 1%, respectively. The related I_{on}, I_{off}, mobility, and V_{th} values are all summarized in Figures 5g and 5h. Note that the $I_{on/off}$ values of the flexible TFTs were all approximately the same, at 4.5×10^5, up to a bending radius of 10 mm, but as the bending radius was decreased under convex bending conditions, the mobility was slightly increased and the V_{th} value was slightly reduced. An opposite trend was observed under concave conditions, with a change in variation of only 4.1%, likely resulting from the amorphous In_2O_3 channel layer being less sensitive to bending conditions. The dependence of V_{th} on strain can be explained by variations in the interatomic distance within the In_2O_3 layer. For instance, in the case of tensile bending, the distance between atoms increases, which leads to a decrease in the splitting of energy levels and, therefore, a narrowing of the band gap.[36] When the band gap is reduced, electrons are more easily excited to the conduction band for the given thermal equilibrium condition. These additional electrons increase the channel conductivity, leading to a negative shift in V_{th}. With compressive bending, on the other hand, a decrease in the interatomic distance causes band-gap widening. This consequently leads to a reduction in channel conductivity and a positive shift in V_{th}. The reversibility of the flexible TFT was also measured after bending to a radius of 10 mm up to 10 000 times (Figure 6), from which it is apparent that the electrical properties remain essentially the same, within an error of 1.3%. On the basis of these results, the operation of a flexible In_2O_3 TFT is considered to be very stable. Nevertheless, its mechanical properties could potentially be improved by adopting strain relief methods such as locating channel materials in a neutral plane by overcoating, or by using an ultrathin substrate.

4. CONCLUSIONS

This study has demonstrated that a solution-processed ZrO_2:B thin film can be applied as both a hydrophobic surface modification layer and inorganic glue in flexible TFTs. Applying this ZrO_2:B layer to a PVP dielectric changes it from hydrophilic to hydrophobic, thus allowing for the deposition of an aqueous In_2O_3 solution and the creation of an integrated and flexible amorphous In_2O_3 TFT. This surface-engineered PVP dielectric exhibits a lower J_{leak} value, while the final ZrO_2:B/PVP dielectric shows experiences no breakdown behavior under a 5-mm bending condition in either the convex or concave direction. Furthermore, the electrical properties of a flexible amorphous In_2O_3 TFT are retained up to a 10-mm bending condition. Therefore, the use of a ZrO_2:B thin film as a surface-modifying inorganic glue layer presents a promising approach to producing flexible TFTs based on a hydrophobic dielectric surface.

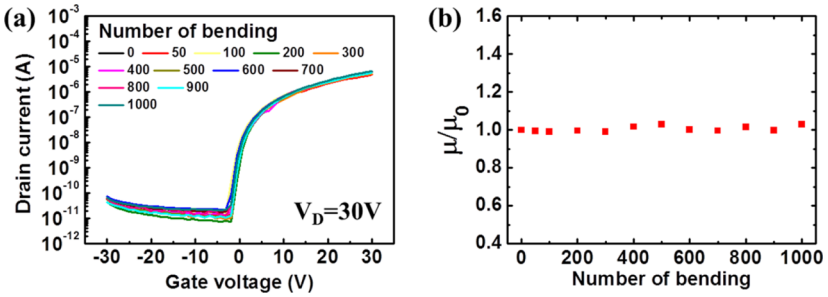

Figure 6. (a) Transfer curves of a flexible In_2O_3 TFT and (b) the change in its mobility values as a function of the number of times bent to a radius of 10 mm.

DOI: 10.1021/acsami.5b00036
ACS Appl. Mater. Interfaces 2015, 7, 4494−4503

■ ASSOCIATED CONTENT

Supporting Information

Binding energies and corresponding phases are summarized in Table S1. The XRD spectra and XPS survey scans of ZrO_2:B layer before and after UVO treatment. Optical and AFM images of ZrO_2:B/PS thin film. Optical and SEM images of PVP, PVP with UVO treatment, and ZrO_2:B/PVP layer. FT-IR results of as-deposited PVP and a cross-linked PVP thin film. XPS data for a ZrO_2:B thin film. AFM images of a PI substrate, PVP planarization layer, PVP dielectric layer, ZrO_2:B surface-modified layer, and In_2O_3 channel layer. SEM images of a ZrO_2:B/PVP and In_2O_3/ZrO_2:B/PVP layer after 5 mm of convex bending. AFM image of an In_2O_3/ZrO_2:B/PVP surface after 5 mm of bending. These materials are available free of charge via the Internet at http://pubs.acs.org.

■ AUTHOR INFORMATION

Corresponding Authors

*Tel.: +82-31-750-8529. E-mail: t2.lee77@gachon.ac.kr (T. I. Lee).

*Tel.: +82-2-2123-2838. E-mail: thinfilm@yonsei.ac.kr (H. K. Baik).

Notes

The authors declare no competing financial interest.

■ ACKNOWLEDGMENTS

This work was supported by the National Research Foundation of Korea (No. NRF-2010-0029207) and Creative Allied Program (ACP-12-1), as funded by the Korea Ministry of Science, ICT & Future Planning (MSIP). Further funding was provided by LG Display.

■ REFERENCES

(1) Jeong, S.; Lee, J.; Lee, S. S.; Seo, Y.; Kim, S.; Park, J.; Ryu, B.; Yang, W.; Moon, J.; Choi, Y. Metal Salt-Derived In-Ga-Zn-O Semiconductors Incorporating Formamide as a Novel Co-Solvent for Producing Solution-Processed, Electrohydrodynamic-Jet Printed, High Performance Oxide Transistors. *J. Mater. Chem. C* **2013**, *1*, 4236−4243.

(2) Lee, K. H.; Park, J. H.; Yoo, Y. B.; Jang, W. S.; Oh, J. Y.; Chae, S. S.; Moon, K. J.; Myoung, J. M.; Baik, H. K. Effects of Solution Temperature on Solution-Processed High-Performance Metal Oxide Thin-Film Transistors. *ACS Appl. Mater. Interfaces* **2013**, *5*, 2585−2592.

(3) Park, J. H.; Choi, W. J.; Oh, J. Y.; Chae, S. S.; Jang, W. S.; Lee, S. J.; Song, K. M.; Baik, H. K. Low-Temperature, Aqueous-Solution-Processed Zinc Tin Oxide Thin Film Transistor. *Jpn. J. Appl. Phys.* **2011**, *50*, 070201.

(4) Meyers, S. T.; Anderson, J. T.; Hung, C. M.; Thompson, J.; Wager, J. F.; Keszler, D. A. Aqueous Inorganic Inks for Low-Temperature Fabrication of ZnO TFTs. *J. Am. Chem. Soc.* **2008**, *130*, 17603−9.

(5) Park, J. H.; Yoo, Y. B.; Lee, K. H.; Jang, W. S.; Oh, J. Y.; Chae, S. S.; Baik, H. K. Low-Temperature, High-Performance Solution-Processed Thin-Film Transistors with Peroxo-Zirconium Oxide Dielectric. *ACS Appl. Mater. Interfaces* **2013**, *5*, 410−417.

(6) Park, J. H.; Yoo, Y. B.; Lee, K. H.; Jang, W. S.; Oh, J. Y.; Chae, S. S.; Lee, H. W.; Han, S. W.; Baik, H. K. Boron-Doped Peroxo-Zirconium Oxide Dielectric for High-Performance, Low-Temperature, Solution-Processed Indium Oxide Thin-Film Transistor. *ACS Appl. Mater. Interfaces* **2013**, *5*, 8067−8075.

(7) Ko, J.; Kim, J.; Park, S. Y.; Lee, E.; Kim, K.; Lim, K. H.; Kim, Y. S. Solution-Processed Amorphous Hafnium-Lanthanum Oxide Gate Insulator for Oxide Thin-Film Transistors. *J. Mater. Chem. C* **2014**, *2*, 1050−1056.

(8) Park, J. H.; Kim, K.; Yoo, Y. B.; Park, S. Y.; Lim, K.; Lee, K. H.; Baik, H. K.; Kim, Y. S. Water Adsorption Effects of Nitrate Ion Coordinated Al_2O_3 Dielectric for High Performance Metal-Oxide Thin-Film Transistor. *J. Mater. Chem. C* **2013**, *1*, 7166−7174.

(9) Kim, G. H.; Shin, H. S.; Ahn, B. D.; Kim, K. H.; Park, W. J.; Kim, H. J. Formation Mechanism of Solution-Processed Nanocrystalline InGaZnO Thin Film as Active Channel Layer in Thin-Film Transistor. *J. Electrochem. Soc.* **2009**, *156*, H7−H9.

(10) Kim, M. G.; Kanatzidis, M. G.; Facchetti, A.; Marks, T. J. Low-Temperature Fabrication of High-Performance Metal Oxide Thin-Film Electronics via Combustion Processing. *Nat. Mater.* **2011**, *10*, 382−388.

(11) Banger, K. K.; Yamashita, Y.; Mori, K.; Peterson, R. L.; Leedham, T.; Rickard, J.; Sirringhaus, H. Low-Temperature, High-Performance Solution-Processed Metal Oxide Thin-Film Transistors Formed by a "Sol−Gel on Chip" Process. *Nat. Mater.* **2011**, *10*, 45−50.

(12) Kim, Y.; Heo, J.; Kim, T.; Park, S.; Yoon, M.; Kim, J.; Oh, M. S.; Yi, G.; Noh, Y.; Park, S. K. Flexible Metal-Oxide Devices Made by Room-Temperature Photochemical Activation of Sol−Gel Films. *Nature* **2012**, *489*, 128−132.

(13) Rim, Y. S.; Jeong, W. H.; Kim, D. L.; Lim, H. S.; Kim, K. M.; Kim, H. J. Simultaneous Modification of Pyrolysis and Densification for Low-Temperature Solution-Processed Flexible Oxide Thin-Film Transistors. *J. Mater. Chem.* **2012**, *22*, 12491−12497.

(14) Song, K.; Jeong, Y.; Jun, T.; Koo, C. Y.; Kim, D.; Woo, K.; Kim, A.; Noh, J.; Cho, S.; Moon, J. Low-Temperature Solution-Deposited Oxide Thin-Film Transistors Based on Solution-Processed Organic−Inorganic Hybrid Dielectrics. *Jpn. J. Appl. Phys.* **2010**, *49*, 05EB02.

(15) Yang, C.; Hong, K.; Jang, J.; Chung, D. S.; An, T. K.; Choi, W.; Park, C. E. Solution-Processed Flexible ZnO Transparent Thin-Film Transistors with a Polymer Gate Dielectric Fabricated by Microwave Heating. *Nanotechnology* **2009**, *20*, 465201.

(16) Lin, Y.; Faber, H.; Zhao, K.; Wang, Q.; Amassian, A.; McLachlan, M.; Anthopoulos, T. D. High-Performance ZnO Transistors Processed Via an Aqueous Carbon-Free Metal Oxide Precursor Route at Temperatures Between 80−180 °C. *Adv. Mater.* **2013**, *25*, 4340−4346.

(17) Lee, C. Y.; Lin, M. Y.; Wu, W. H.; Wang, J. Y.; Chou, Y.; Su, W. F.; Chen, Y. F.; Lin, C. F. Flexible ZnO Transparent Thin-Film Transistors by a Solution-Based Process at Various Solution Concentrations. *Semicond. Sci. Technol.* **2010**, *25*, 105008.

(18) Bong, H.; Lee, W. H.; Lee, D. Y.; Kim, B. J.; Cho, J. H.; Cho, K. High-Mobility Low-Temperature ZnO Transistors with Low-Voltage Operation. *Appl. Phys. Lett.* **2010**, *96*, 192115.

(19) Jung, Y.; Jun, T.; Kim, A.; Song, K.; Yeo, T. H.; Moon, J. Direct Photopatternable Organic−Inorganic Hybrid Gate Dielectric for Solution-Processed Flexible ZnO Thin Film Transistors. *J. Mater. Chem.* **2011**, *21*, 11879−11885.

(20) Wong, H. S. P.; Frank, D. J.; Solomon, P. M.; Wann, C. H. J.; Welser, J. J. Nanoscale CMOS. *Proc. IEEE* **1999**, *87*, 537−570.

(21) Nicollian, E. H.; Berglund, C. N.; Schmidt, P. F.; Andrews, J. M. Electrochemical Charging of Thermal SiO_2 Films by Injected Electron Currents. *J. Appl. Phys.* **1971**, *42*, 5654.

(22) Olthuis, W.; Bergveld, P. On the Charge Storage and Decay Mechanism in Silicon Dioxide Elecrets. *IEEE Trans. Electr. Insul.* **1992**, *27*, 691−697.

(23) Yoon, J. Y.; Kim, Y. H.; Ka, J. W.; Hong, S. K.; Yia, M. H.; Jang, K. S. A High-Temperature Resistant Polyimide Gate Insulator Surface-Modified with a YO_x Interlayer for High-Performance, Solution-Processed Li-doped ZnO Thin-Film Transistors. *J. Mater. Chem. C* **2014**, *2*, 2191−2197.

(24) Yoo, S.; Yoon, J. Y.; Ryu, J.; Kim, Y. H.; Ka, J. W.; Yi, M. H.; Jang, K. S. Low-Temperature-Annealed Alumina/Polyimide Gate Insulators for Solution-Processed ZnO Thin-Film Transistors. *Appl. Surf. Sci.* **2014**, *313*, 382−388.

(25) Son, B. G.; Je, S. Y.; Kim, H. J.; Jeong, J. K. Modification of a Polymer Gate Insulator by Zirconium Oxide Doping for Low

DOI: 10.1021/acsami.5b00036
ACS Appl. Mater. Interfaces 2015, 7, 4494−4503

Temperature, High Performance Indium Zinc Oxide Transistors. *RSC Adv.* **2014**, *4*, 45742−45748.
(26) Kim, K.; Lee, E.; Kim, J.; Park, S. Y.; Lim, K.; Shin, C.; Kim, Y. S. Interface Engineering for Suppression of Flat-Band Voltage shift in a Solution-Processed ZnO/Polymer Dielectric Thin Film Transistor. *J. Mater. Chem. C* **2013**, *1*, 7742−7747.
(27) Yang, W.; Song, K.; Jung, Y.; Jeong, S.; Moon, J. Solution-Deposited Zr-doped AlO_x Gate Dielectrics Enabling High-Performance Flexible Transparent Thin Film Transistors. *J. Mater. Chem. C* **2013**, *1*, 4275−4282.
(28) Hwang, D. K.; Kim, C. S.; Choi, J. M.; Lee, K.; Park, J. H.; Kim, E.; Baik, H. K.; Kim, J. H.; Im, S. Polymer/YO_x Hybrid-Sandwich Gate Dielectrics for Semitransparent Pentacene Thin-Film Transistors Operating Under 5 V. *Adv. Mater.* **2006**, *18*, 2299−2303.
(29) Socrates, G. *Infrared Characteristic Group Frequencies: Tables and Charts*, 3rd Edition; John Wiley & Sons: New York, 1994; Vol. 6, p 94.
(30) Valov, I.; Stoychev, D.; Marinova, T. Study of the Kinetics of Processes During Electrochemical Deposition of Zirconia from Nonaqueous Electrolytes. *Electrochim. Acta* **2002**, *47*, 4419−4431.
(31) Park, J.; Heo, J. K.; Kang, Y. The Properties of RF Sputtered Zirconium Oxide Thin Films at Different Plasma Gas Ratio. *Bull. Korean Chem. Soc.* **2010**, *31*, 397−400.
(32) Harnchana, V.; Hindmarch, A. T.; Sarahan, M. C.; Marrows, C. H.; Brown, A. P.; Brydson, R. M. D. Evidence for Boron Diffusion into Sub-Stoichiometric MgO(001) Barriers in CoFeB/MgO-Based Magnetic Tunnel Junctions. *J. Appl. Phys.* **2013**, *113*, 163502.
(33) Liu, S.; Chen, Y.; Chen, H. Studies of Spectroscopy and Cyclic Voltammetry on a Zirconium Hexacyanoferrate Modified Electrode. *J. Electroanal. Chem.* **2001**, *502*, 197−203.
(34) Liu, J.; Buchholz, D. B.; Hennek, J. W.; Chang, R. P. H.; Facchetti, A.; Marks, T. J. All-Amorphous-Oxide Transparent, Flexible Thin-Film Transistors. Efficacy of Bilayer Gate Dielectrics. *J. Am. Chem. Soc.* **2010**, *132*, 11934−11942.
(35) Snow, E. H.; Grove, A. S.; Deal, B. E.; Sah, C. T. Ion Transport Phenomena in Insulating Films. *J. Appl. Phys.* **1965**, *36*, 1664−1673.
(36) Uchida, K.; Krishnamohan, T.; Saraswat, K. C.; Nishi, Y. Physical Mechanisms of Electron Mobility Enhancement in Uniaxial Stressed MOSFETs and Impact of Uniaxial Stress Engineering in Ballistic Regime. *IEDM Technol. Dig.* **2005**, 129−132.
(37) Senthilnathan, J.; Weng, C.-C.; Liao, J.-D.; Yoshimura, M. Submerged Liquid Plasma for the Synthesis of Unconventional Nitrogen Polymers. *Sci. Rep.* **2013**, *3*, 2414−2420.
(38) Dicke, C.; Morstein, M.; Hahner, G. Surface Inorganic Chemistry: the Reaction of Hydroxyl-Terminated Thiols on Gold with a Zirconium Coordination Compound. *Langmuir* **2002**, *18*, 336−344.
(39) Ago, H.; Kugler, T.; Cacialli, F.; Salaneck, W. R.; Shaffer, M. S. P.; Windle, A. H.; Friend, R. H. Work Functions and Surface Functional Groups of Multiwall Carbon Nanotubes. *J. Phys. Chem. B* **1999**, *103*, 8116−8121.
(40) Zhou, K.; Wu, X.; Zhang, X.; Qin, L.; Liao, B. Effect of the C_2H_2 and N_2 Flow Rate on Nanocomposite nc-ZrCN/a-C:H(N) Film Synthesized by Filtered Cathodic Vacuum Arc Technique. *Surf. Rev. Lett.* **2008**, *15*, 781−786.
(41) Yan, X.; Xu, T.; Chen, G.; Yang, S.; Liu, H. Study of Structure, Tribological Properties and Growth Mechanism of DLC and Nitrogen-Doped DLC Films Deposited by Electrochemical Technique. *Appl. Surf. Sci.* **2004**, *236*, 328−335.

DOI: 10.1021/acsami.5b00036
ACS Appl. Mater. Interfaces 2015, 7, 4494−4503